# X-ray and Electrochemical Studies of Cu UPD on Au(111) Single-Crystal Electrodes in the Presence of Bromide

**Enrique Herrero,† Samantha Glazier, and Héctor D. Abruña***

*Department of Chemistry, Baker Laboratory, Cornell University, Ithaca, New York 14853-1301*

*Received: May 11, 1998; In Final Form: July 16, 1998*

The underpotential deposition (UPD) of copper on Au(111) in the presence of bromide anions has been investigated employing electrochemical techniques, in-situ grazing incidence X-ray diffraction (GIXD), and crystal truncation rod (CTR) measurements. At potentials positive of +0.55 V (vs Ag/AgCl), bromide adsorbs on the electrode surface forming an ordered and rotated hexagonal structure. The rotation angle of this structure with respect to the Au(01) direction and the Br−Br distance change with the applied potential. At potentials below +0.55 V, the bromide overlayer becomes disordered although its coverage remains high. The initial stages of copper deposition (at ca. +0.36 V) lower the gold's work function, giving rise to an increase in the bromide coverage and the formation of an ordered bromide layer with a coverage of 0.51. At +0.32 V there is a sharp voltammetric feature that corresponds to a phase transition to give a (4 × 4) bromide layer with a coverage of 0.563. Over the potential range from +0.32 to ca. +0.20 there are two voltammetric features associated with additional copper deposition, giving rise to a stoichiometric CuBr layer. At +0.147 V there is another sharp voltammetric feature which, again, is ascribed to a phase transition giving rise to a (1 × 1) copper layer with a bromide (4 × 4) structure adsorbed over the copper layer. At this potential, the distances between the bromide and copper layers are similar to those found in solid CuBr. At potentials negative of +0.147 V, bulk copper deposition begins.

## 1. Introduction

The UPD (underpotential deposition)[1,2] of metals onto foreign metal substrates provides an excellent means for studying the interactions between the different solution components and the metal surface, as well as the different factors that modify such interactions. The use of single-crystal surfaces in conjunction with in-situ surface techniques, including STM,[3−6] AFM,[7,8] and surface X-ray-based techniques,[8−13] has allowed a detailed investigation of UPD processes, allowing the separation of the contributions of the different interactions to the global UPD process. Three main interactions can be considered in UPD processes: (i) depositing metal−electrode surface, (ii) anion−depositing metal, and (iii) anion−electrode surface. From these three interactions, the main driving force for the UPD process is generally the depositing metal−electrode surface interaction.

However, the other two interactions can also play important roles. The presence of strongly adsorbing anions in the electrolyte has particular importance, since the anion−metal and anion−substrate interactions can significantly modify UPD processes. Anions, such as chloride, have been shown to form stable bilayers on electrode surfaces where the metal adatom is generally sandwiched between the electrode surface below and the anion adlayer above.[9,14] In these cases, the strong interaction between the metal and the anion plays an essential role in bilayer formation. Such strong anion−metal interactions often result in the formation of ordered structures similar to those present in the corresponding halide salt of the metal being deposited.[14]

Regarding the interactions with the electrode surface, its surface properties continuously change since a foreign metal is being deposited during the UPD process. This can lead to a change in the adsorption properties of the electrode surface during the UPD process. For Pt(111) electrodes, small amounts of UPD copper induce changes in the electrodes' surface properties so that an enhancement of the chloride adsorption is observed.[15] Similarly, the presence of copper electrodeposited on step sites (of stepped surfaces) enhances the adsorption of sulfate on neighboring platinum sites.[16]

The UPD of Cu on Au(111) in sulfate media represents one of the most widely studied and better characterized systems. Deposition takes place in two distinct steps where the first is a honeycomb lattice structure ($\theta = {}^2/_3$) and the second is a commensurate full monolayer ($\theta = 1$). The effects of other anions have received significantly less attention.

In this paper we present a study of the UPD of Cu on Au(111) in the presence of bromide anions. We have employed electrochemical and in-situ X-ray techniques (grazing incident X-ray diffraction (GIXD) and crystal truncation rod (CTR) measurements). These techniques provide complementary information for a more detailed understanding of the different interactions present.

## 2. Experimental Section

X-ray diffraction experiments were performed at the X20-C beamline at the National Synchrotron Light Source using a four-circle diffractometer. On this beamline, radiation from a bending magnet of the electron storage ring was focused with a Pt-coated bent cylindrical mirror and monochromatized with a double-Si(111) monochromator. X-ray photons of 1.4067 Å wavelength were employed. A reflection geometry sample cell similar to those used in previous studies[17−19] was employed. X-ray photons penetrate through a 2.5 $\mu$m Mylar film (Chemp-

* Correponding author.
† Present address: Departamento de Química Física, Universidad de Alicante, Spain.

10.1021/jp982192e CCC: $15.00 
Published on Web 08/25/1998

lex) as well as a thin film of electrolyte (estimated to be about 30 $\mu$m) covering the Au(111) crystal. To prevent the diffusion of oxygen from air through the Mylar film, an outer shield with a Kapton window (Chemplex) was placed on top of the sample cell and continuously flushed with ultrapure $N_2$. Cyclic voltammograms in the X-ray cell were carried out with the Mylar film inflated by filling with additional electrolyte solution. For X-ray measurements, part of the electrolyte was removed so that the Mylar film was tightly pressed against the crystal surface, achieving a thin-layer configuration.

The X-ray reflections are referred to the hexagonal coordinates of the Au(111) substrate with $\mathbf{a}_s$ and $\mathbf{b}_s$ along the nearest-neighbor direction in the surface plane ($a_s = b_s = 2.885$ Å) and $\mathbf{c}_s$ ($c_s = 2.3556$ Å) normal to the surface. Grazing incidence X-ray diffraction (GIXD) measurements were carried out in the azimuth fixed mode where the incident and outgoing angles were kept small ($\alpha = \beta \approx 3.5°$, $L = 0.1$ reciprocal lattice units (rlu)) so as to reduce the background and the absorption by the Mylar film and water solution.

Specular crystal truncation rod (CTR) measurements were carried out across the (00*L*) Bragg diffraction points. A complete CTR measurement consists of a series of surface rocking curves at $Q_z$ ranging from 0 to 2 rlu. Each rocking curve was fitted to a Lorentzian line shape to derive the integrated intensity, which was subsequently used for fitting with a model consisting of atomic layers along the surface normal. Each layer is described by three parameters: the coverage $\Theta_n$ (defined as the atomic ratio of the species in the *n*th layer to that of Au atoms in a bulk Au(111) layer), the atomic root-mean-square (rms) displacement $\sigma_n$, and the interlayer distance $d$ (from the *n*th layer to the $(n-1)$th layer). These values were fixed at $\Theta_n = 1$, $\sigma_n = 0.085$ Å, and $d = 2.3556$ Å as reported for bulk Au(111) layers.[20] In addition to the bulk Au(111) layers, three different layers are considered: the topmost Au(111) layer, with a fixed $\Theta_0 = 1$ but with variable $\sigma$ and $d$, and two adsorbate layers. The atomic scattering factors were numerically calculated from the empirical equations in the International Tables for Crystallography.[21] A full description of the fitting model has been given elsewhere.[20,22]

Electrochemical and X-ray measurements were carried out with Au(111) electrodes with a miscut of less than 0.3°. Prior to any measurement, electrodes were flame-annealed, quenched with ultrapure water,[23] and transferred to the cell for the electrochemical and the X-ray measurements.

All potentials were measured versus a Ag/AgCl electrode in 3 M NaCl. A large area coiled gold or platinum wire was used as a counter electrode in both the electrochemical and X-ray cells. Coverages are defined as the atomic ratio of the species in the particular layer to that of Au atoms in a bulk Au(111) layer. All experiments were carried out at room temperature. Solutions were prepared using ultrapure water (18 Mohm Millipore Milli-Q water), $H_2SO_4$ (Ultrex J. T. Baker), $HClO_4$ (Ultrex J. T. Baker), CuO (99.9999%, Aldrich), and NaBr (99.99%, Aldrich).

## 3. Results and Discussion

Figure 1 shows the voltammetric profile of a Au(111) electrode immersed in 0.1 M $HClO_4$ + 1.0 mM NaBr + 1.0 mM $Cu^{2+}$, which presents four different peaks. From these, two of them, peaks I and IV, are especially sharp and define three regions in the voltammetric profile as shown in Figure 1. We have studied the different processes taking place on the electrode surface in each region by electrochemical and in-situ X-ray methods (GIXD and CTR measurements). Since the

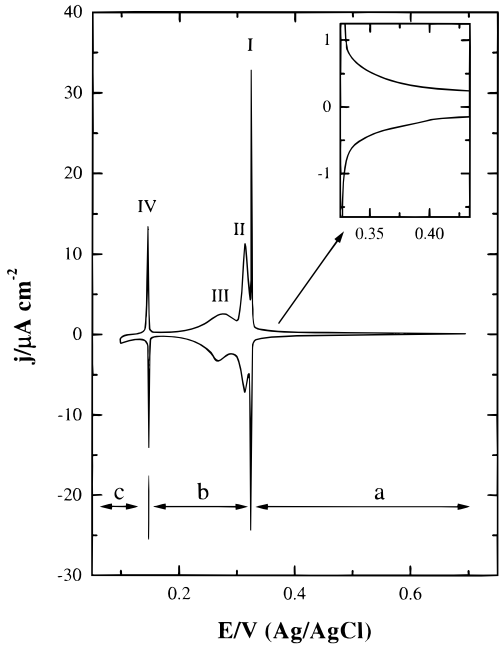


**Figure 1.** Voltammetric profile of a Au(111) electrode in contact with a 0.1 M $HClO_4$ + 1.0 mM NaBr + 1.0 mM $Cu^{2+}$ solution in the electrochemical cell. The different regions selected for study are marked with the arrows. Scan rate: 1 mV $s^{-1}$.

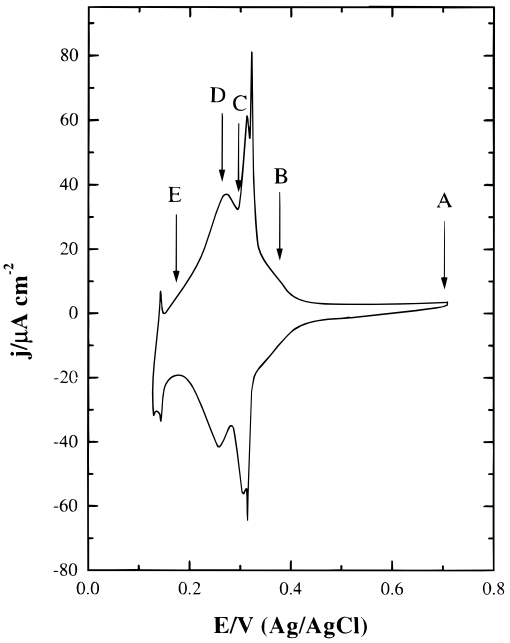


**Figure 2.** Voltammetric profile of a Au(111) electrode in contact with a 0.1 M $HClO_4$ + 1.0 mM NaBr + 1.0 mM $Cu^{2+}$ solution in the X-ray cell. The arrows indicate the potentials at which the CTR measurements were taken. Scan rate: 5 mV $s^{-1}$.

geometry of the X-ray cell is different form that of the normal electrochemical cell, the voltammetric profile obtained in the X-ray cell is presented in Figure 2. Due to the contributions from the sides of the electrode, which are polycrystalline, and the intrinsic *iR* drops in the X-ray cell, the double layer is wider and the peaks are less sharp. However, the four peaks characteristic of Cu UPD on Au(111) electrodes in the presence of bromide are still clearly visible with no additional voltametric peaks present, ensuring the cleanliness of the X-ray cell. The arrows in Figure 2 mark the positions where the CTRs were taken. Prior to any surface X-ray measurement, the quality of the Au(111) surface was checked by GIXD (Figure 3). The

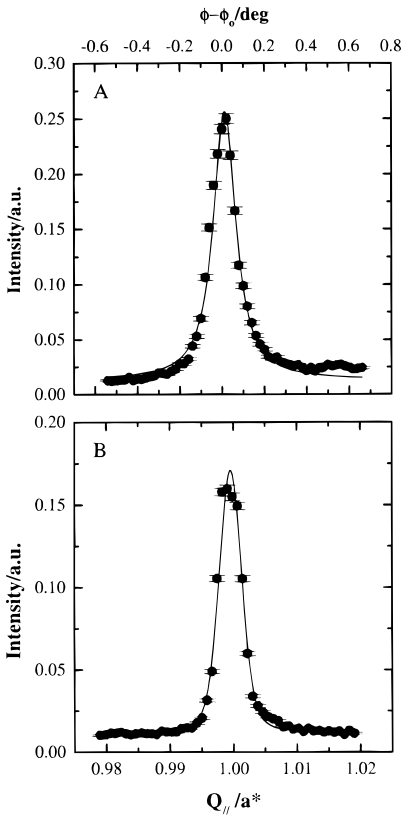


**Figure 3.** In-plane (A) radial and (B) azimuthal scans of the Au(111) surface diffraction, fitted to Lorentzians (solid line).

presence of well-defined Au(111) surface peaks ensures that the surface has not been disordered during either the electrode treatment or the Cu UPD process. From the azimuthal scan in Figure 3A, a correlation length of 1270 Å was obtained. This, however, represents a lower limit since it was limited by the detector slits.

**3.1. Region a.** This region comprises all the processes taking place at potentials positive of peak I (present at +0.324 V in this medium). From the voltammetric point of view, no significant processes appear to take place in this region. The only significant currents are observed at potentials close to peak I (shown in the inset to Figure 1 and more clearly in Figure 2), probably associated with the onset of the UPD process. This shoulder is similar to that found for Cu UPD on Au(111) electrodes in sulfuric acid.[24] In this latter case, the shoulder was associated with the adsorption of the anion ((bi)sulfate) and Cu on the electrode surface.

Assuming that the Cu UPD process begins at the shoulder of peak I, one would anticipate that the behavior of the electrode at potentials above this value would be the same as that obtained in the absence of copper in solution for the same bromide concentration. Previous work by Ocko et al. has shown that, on Au(111) surfaces, bromide anions (at the same solution concentration) adsorb at potentials above +0.55 V, forming an incommensurate hexagonal structure.[25,26] This structure is rotated relative to the Au(111) surface at an angle that depends on the electrode potential. Moreover, the Br−Br distance compresses when the potential in made more positive. Therefore, the same ordered structure should be observable under the present conditions, again assuming that the shoulder in the voltammogram corresponds to the onset of copper UPD.

Figure 4 presents a radial scan for the diffraction peak found at +0.70 V. This peak is rotated 26.8° with respect to the (10) direction, as shown in Figure 5(open squares). Due to the

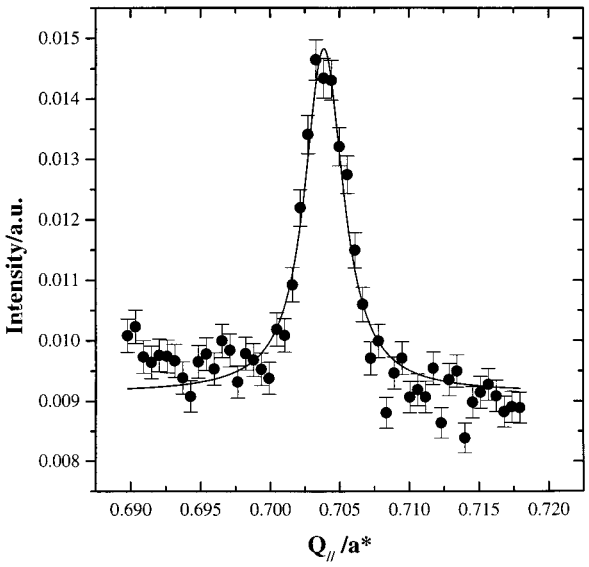


**Figure 4.** In-plane radial scan of the diffraction peak of the bromide overlayer found at +0.70 V, fitted to a Lorenztian (solid line).

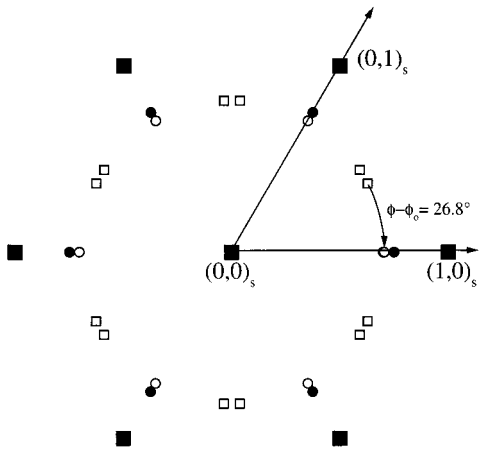


**Figure 5.** Reciprocal space map of the in-plane diffraction peaks from the Au(111) surface (■), the rotated hexagonal bromide overlayer at +0.70 V (□), the hexagonal overlayer found between +0.36 and +0.32 V (○), and the (4 × 4) structure found between +0.32 and +0.10 V (●).

hexagonal symmetry of the surface, another peak is found at a rotation angle from (01) of 33.2°. The position of these surface peaks and their potential dependence are in good agreement with the previously mentioned work of Ocko et al. in the absence of Cu.[26] This fact clearly indicates that the presence of copper ions in solution has no effect at these potential values and that the UPD process starts at more negative potentials.

Surface charge effects can explain the compression, with increasing potential, of this surface structure. At +0.70 V, a value well above the pzc of gold for this surface,[27] the electrode surface has a positive charge. Increasing potentials will increase the positive charge on the electrode, attracting the bromide anions more strongly to the electrode surface. For this structure, the Br−Br distance found, 4.102 Å (Table 1), is larger than the van der Waals diameter of the bromide (3.70−4.00 Å) anion,[28] and therefore some additional compression in the structure is possible, allowing for an increase in the bromide surface coverage.

The specular CTR measurements taken at this potential (+0.70 V) provide information about the coverage of the bromide layer, the distance between the bromide layer and the topmost Au layer, and the expansion of this latter layer with

**TABLE 1: Stability Range, Bromide Coverage, and Br−Br Distance for the Different Ordered Structures Obtained from the GIXD Measurements**

| structure | stability range | $\Theta_{Br}$ | Br−Br distance/Å |
|---|---|---|---|
| rotated hexagonal | $E > +0.60$ V | 0.495 | 4.102 |
| hexagonal (pseudo-(4 × 4)) | $+0.36 > E > +0.32$ V | 0.50−0.54 | 4.08−3.93 |
| (4 × 4) | $E < +0.32$ V | 0.563 | 3.85 |

respect to the bulk Au(111). Figure 6A shows the CTR measurements profile at +0.70 V. As can be seen, the valleys in the CTR curve are deeper than those in the ideally terminated Au(111) surface (dashed line), a clear indication of the presence of an adsorbate layer on the electrode surface. In the present case, the CTR profile was fitted using only one overalyer composed of bromide anions. The values obtained from the fitting are listed in Table 2.

The bromide coverage obtained (0.56, see Table 2) is slightly higher than that obtained from the GIXD measurements. The correlation length obtained from the width of the diffraction peak is 400 Å. Therefore, the domain size of the bromide adlayer is much smaller than the surface Au(111) domain size, 1,270 Å. Moreover, the integrated intensity for the diffraction peak is much lower than that obtained for other bromide surface structures with similar coverage, suggesting the presence of disordered domains on the surface. As mentioned above, the Br−Br distance in this layer is larger than the van der Waals diameter so that additional compression is possible. The presence of disordered domains between the ordered domains can explain the difference in coverage obtained form the GIXD and the CTR measurements. These disordered domains will have a slightly higher coverage than the ordered domains, increasing the total coverage. Whereas CTR measurements would be sensitive to this, GIXD would not, thus accounting for the difference.

No other structure was found between +0.55 and +0.38 V. However, at +0.36 V a new structure with a surface diffraction peak at (0.708, 0) was found (Figures 7A and 8A). The complementary peak at (0, 0.708) as well as the second-order diffraction peak were also found. This diffraction feature corresponds to an incommensurate hexagonal structure, close to a (4 × 4) structure (Figure 5, open circles). For this incommensurate structure, the interatomic distance was 4.08 Å with a coverage of 0.501 (Table 1). Moreover, this structure compresses when the potential is moved negatively. At +0.34 V, an interatomic distance of 3.93 Å is obtained which, in turn, gives a coverage value of 0.538 (Figures 7B and 8B).

The azimuthal scan gives a correlation length of ca. 1000 Å, slightly smaller than the resolution limit. The domain size in this case is larger than that obtained for the rotated hexagonal structure, and the integrated intensity is much higher than the one obtained at +0.70 V, suggesting a more ordered adlayer. While the azimuthal scan provides information about the domain size, the radial scan gives information about the interatomic distances. In the present structure, the interatomic distance in the different ordered domains is not the same. The radial scan obtained at these potential values shows multiple peaks (Figure 8A,B) that can be fitted with at least three Lorentzian curves. This indicates the presence of different interatomic distances in different domains; i.e., the domains exhibit a different degree of compressibility at a given potential over this range.

In principle, if we consider that the shoulder of peak I (Figure 1, inset) represents the onset of Cu UPD, the structure found can have three different compositions: it could be composed entirely of bromide, of copper alone, or of a copper−bromide species. In all cases, the coverage of one of the adsorbed species on the electrode surface would have to be close to 0.50, as determined by GIXD. To identify the composition of the ordered structure, results from the CTR measurements were employed.

The CTR measurement taken at +0.36 V is presented in Figure 6B. From the three possible overlayer compositions presented above, only the model consisting of a bromide layer gave CTR results consistent with the GIXD measurements (Table 2). The introduction of an additional copper layer did not improve the fitting, and the copper coverage values obtained were very low. These low values are consistent with the assumption that the shoulder of peak I represents the onset of the copper deposition process. The charge under this peak is not sufficient to justify the presence of a copper adlayer with a coverage value of ca. 0.50. The bromide coverage obtained is, within experimental error, the same as the one obtained by GIXD, indicating that the ordered bromide layer covers the entire electrode surface and that disordered domains are not present at this potential value.

This model in which the overlayer, on the electrode surface, is composed of a bromide layer with a coverage of 0.50−0.51 and a very low copper coverage is consistent with the chronocoulometric data obtained by Lipkowski et al.,[29−31] who showed that the bromide coverage (even in the absence of copper in solution) is relatively high at potentials above +0.00 V.[30] This is in agreement with the voltammetric results that show a very small charge exchanged in the region between +0.33 and +0.70 V (Figure 1, inset) and the GIXD and CTR measurements that give coverage values of the bromide layer of around 0.50. Moreover, variations in the bromide surface concentration in the presence of copper cations obtained by chronocoulometry[29−31] are very similar to those obtained here. From +0.35 to +0.28 V, the bromide coverage increased from 0.45 to 0.58 and remained constant for potentials below +0.28 V.[31] Those measurements also showed that the copper coverage changed from essentially 0 at +0.37 V to about 0.10 at +0.32 V,[31] corroborating our results obtained from CTR measurements that the copper coverage is very low (almost negligible) at +0.37 V.

Unlike the rotated hexagonal structure that exhibited a compression in the Br−Br distance when the potential was made more positive, the structure found between +0.32 and +0.36 V compresses when the potential is made more negative. Therefore, charge effects cannot explain the compression observed. In fact, the bromide coverage obtained at these lower potential values is higher than that at +0.70 V, when the electrode charge in much more positive. Some additional effect has to be considered in order to explain the presence of this structure at these potential values and the observed compression. This structure was not observed when copper was not present in solution.[25,26] Thus, a copper species must be involved in the formation of this ordered structure. From chronocoulometric measurements it is known that copper is present at low coverage on the electrode surface between +0.32 and +0.37 V, suggesting that this low level of copper on the electrode surface can significantly change the coverage of the anion by enhancing its adsorption. Such enhancement in the adsorption of anions has been previously observed for copper deposited on platinum electrodes. On Pt(111) electrodes, small amounts of UPD copper enhance the adsorption of chloride and bromide,[15] and copper deposited on stepped platinum surfaces can enhance the adsorption of (bi)sulfate.[16] In these two previous cases, the

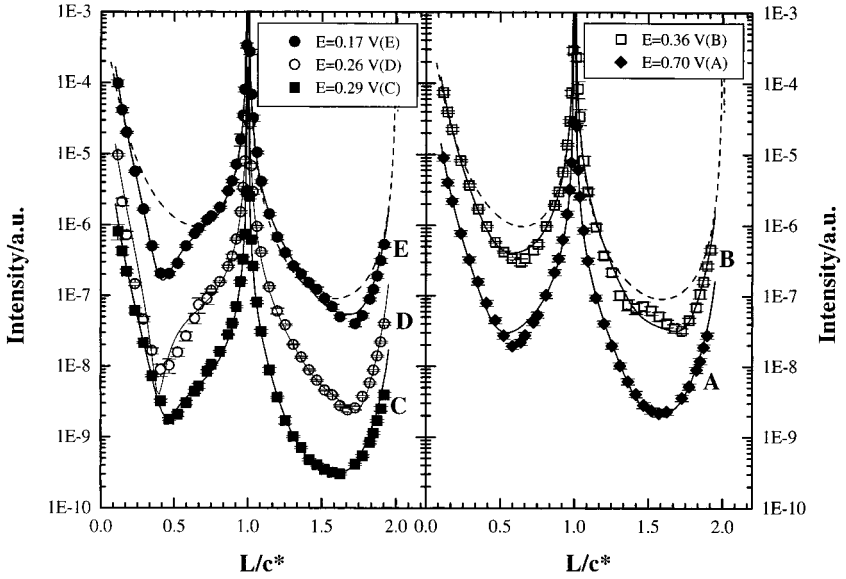


**Figure 6.** CTR measurements of a Au(111) electrode with a 0.1 M $HClO_4$ + 1.0 mM NaBr + 1.0 mM $Cu^{2+}$ solution at (A) $E = +0.70$ V (◆), (B) $E = +0.36$ V (□), (C) $E = +0.29$ V (◆), (D) $E = +0.26$ V (○), and (E) $E = +0.17$ (●). The dashed line is the calculated CTR curve for an ideally truncated Au(111) crystal. The continuous lines are the fits to the experimental data. (A) and (D) are shifted by 1 order of magnitude and (C) by 2 orders of magnitude for a clearer view.

**TABLE 2: Specular CTR Fitting Parameters in a 0.1 M $HClO_4$ + 1.0 mM NaBr + 1.0 mM $Cu^{2+}$ Solution at Different Potentials, Where $\Theta_n$ Is Defined as the Atomic Ratio of the Species in the *n*th Layer to That of Au Atoms in a Bulk Au(111) Layer, $\sigma_n$ Is the Atomic Root-Mean-Square Displacement, and $d_n$ Is the Interlayer Distance from the *n*th Layer to the $(n-1)$th Layer**

| *E*/V | $\Theta_{Br}$ from GIXD | Au(111) topmost layer | first layer | second layer |
|---|---|---|---|---|
| +0.70 | 0.495 | $\Theta_0 = 1$ | $\Theta_{Br} = 0.56 \pm 0.03$ | |
| | | $\sigma_0 = 0.144 \pm 0.007$ | $\sigma_{Br} = 0.15 \pm 0.03$ | |
| | | $d_0 = 2.316 \pm 0.002$ Å | $d_1 = 2.42 \pm 0.02$ Å | |
| +0.36 | ≈0.51 | $\Theta_0 = 1$ | $\Theta_{Br} = 0.48 \pm 0.02$ | |
| | | $\sigma_0 = 0.125 \pm 0.006$ | $\sigma_{Br} = 0.11 \pm 0.03$ | |
| | | $d_0 = 2.290 \pm 0.007$ Å | $d_1 = 2.44 \pm 0.03$ Å | |
| +0.29 | 0.563 | $\Theta_0 = 1$ | $\Theta_{Cu} = 0.37 \pm 0.05$ | $\Theta_{Br} = 0.563$ |
| | | $\sigma_0 = 0.15 \pm 0.01$ | $\sigma_{Cu} = 0.12 \pm 0.07$ | $\sigma_{Br} = 0.36 \pm 0.07$ |
| | | $d_0 = 2.316 \pm 0.005$ Å | $d_1 = 2.43 \pm 0.03$ Å | $d_2 = 0.20 \pm 0.14$ Å |
| +0.26 | 0.563 | $\Theta_0 = 1$ | $\Theta_{Cu} = 0.85 \pm 0.06$ | $\Theta_{Br} = 0.563$ |
| | | $\sigma_0 = 0.17 \pm 0.01$ | $\sigma_{Cu} = 0.12 \pm 0.07$ | $\sigma_{Br} = 0.27 \pm 0.03$ |
| | | $d_0 = 2.355 \pm 0.002$ Å | $d_1 = 2.19 \pm 0.02$ Å | $d_2 = 1.16 \pm 0.05$ Å |
| +0.17 | 0.563 | $\Theta_0 = 1$ | $\Theta_{Cu} = 1$ | $\Theta_{Br} = 0.563$ |
| | | $\sigma_0 = 0.22 \pm 0.01$ | $\sigma_{Cu} = 0.51 \pm 0.03$ | $\sigma_{Br} = 0.15 \pm 0.03$ |
| | | $d_0 = 2.363 \pm 0.002$ Å | $d_1 = 1.85 \pm 0.04$ | $d_2 = 1.57 \pm 0.03$ Å |

enhancement in anion adsorption ostensibly took place in the vicinity of the deposited copper atoms. In the present case, the presence of small amounts of UPD copper induces an increase in the adsorption of bromide with the formation of an ordered layer. The driving force for this enhanced adsorption, on both Pt(111) and Au(111), is likely the lowering of the work function of the substrate that always accompanies the UPD process. Copper has a lower work function than platinum and gold,[32] and small amounts of deposited copper lower the work function of the surface. A lower work function causes a displacement of the pzc of the electrode surface toward negative values, and this, in turn, results in an increase of the positive charge on the surface, thus enhancing anion adsorption. On Au(111) electrodes, the bromide coverage is already high at potentials at the onset of Cu deposition. The diminution of the work function will give rise to an increase in the anion adsorption, with the formation of an ordered structure, thus providing additional stability to the bromide layer.

It is worth noting that the presence of copper also affects the disposition of the bromide layer. At potentials above +0.55 V, the hexagonal bromide layer is rotated 26°−28° from the Au(01) direction, whereas at the onset of Cu UPD the hexagonal bromide layer is completely aligned with the Au(111) surface. However, the distance between the bromide layer and the Au(111) surface and the rms displacement are not affected by this change in the structure (Table 2).

**3.2. Region b.** Region b extends over the range of potentials that includes the very sharp voltammetric peaks at +0.324 and +0.146 V. Very sharp and well-defined voltammetric peaks, such as those mentioned above, are normally associated with phase transitions on the electrode surface, and we shall examine them by GIXD, within that context.

Coinciding with the appearance of peak I at +0.324 V, a significant change in the surface structure is observed by GIXD measurements. The bromide adlayer, which at potentials above +0.32 V was incommensurate, becomes commensurate, giving diffraction peaks at ($^3/_4$, 0) (Figures 7C and 8C). This structure, which can also be referred to as (4 × 4), has the diffraction peaks in reciprocal space depicted in Figure 5 as closed circles. It has a coverage of $^9/_{16}$ (0.563) and an interatomic distance of 3.85 Å (Table 1). This structure is stable throughout region b and, as before, is associated with the bromide layer. The charge measured under peak I cannot justify a significant change in the surface coverage of any of the other surface species involved

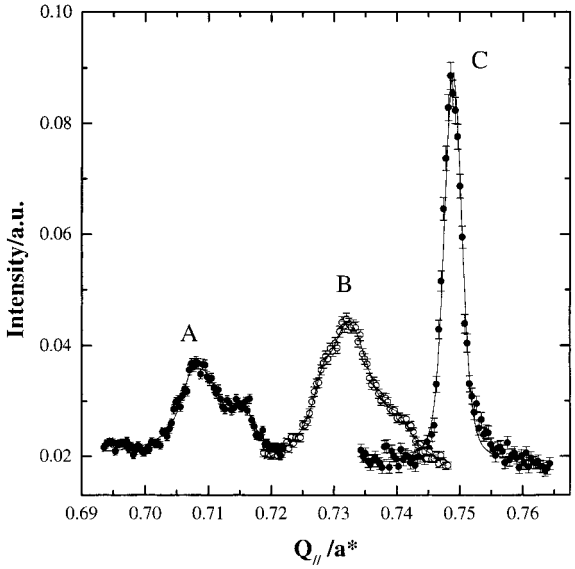


**Figure 7.** In-plane radial scan of the diffraction peak of the overlayer found at (A) +0.36 V, (B) +0.34 V, and (C) between +0.32 and +0.10 V.

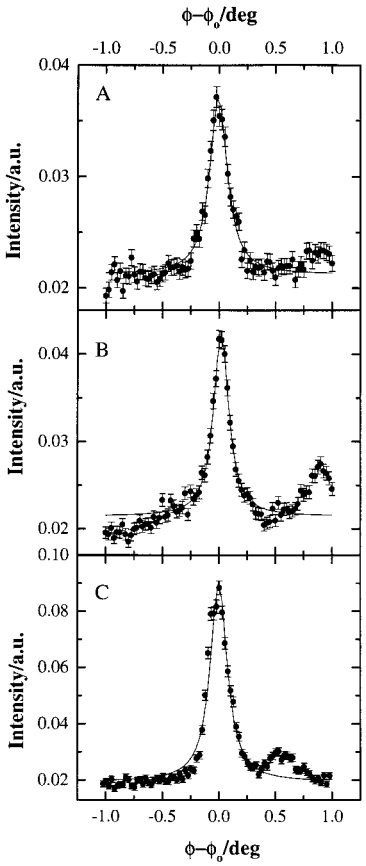


**Figure 8.** In-plane azimuthal scan of the diffraction peak for the overlayer found at (A) +0.36 V, (B) +0.34 V, and (C) between +0.32 and +0.10 V.

in the overlayer and thus has to be associated with the small change in bromide coverage from 0.51 at +0.34 V to 0.563 at +0.32 V.

The transition from the incommensurate to the commensurate (4 × 4) structure precisely matches the potential at which peak I appears, making it responsible for the phase transition in the bromide adlayer. The phase transition between the commensurate and the incommensurate structure is completely

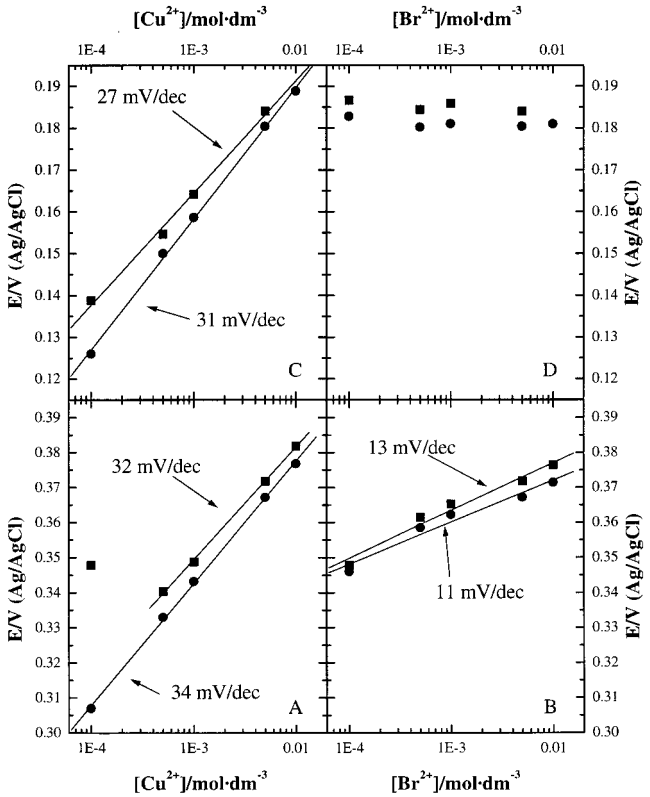


**Figure 9.** (A) Potential for peak I vs copper concentration in 0.1 M $HClO_4$ + 5 × $10^{-3}$ M $Br^-$, (B) potential for peak I vs bromide concentration in 0.1 M $HClO_4$ + 5 × $10^{-3}$ M $Cu^{2+}$, (C) potential for peak IV vs copper concentration in 0.1 M $HClO_4$ + 5 × $10^{-3}$ M $Br^-$, and (D) potential for peak IV vs bromide concentration in 0.1 M $HClO_4$ + 5 × $10^{-3}$ M $Cu^{2+}$. (■) Anodic peak and (●) cathodic peak.

reversible; that is, it always takes place at the same potential (+0.32 V) regardless of the direction of the transformation, suggesting a process that is kinetically rapid.

The diffraction peaks of the commensurate and incommensurate structures exhibit one main difference. In the azimuthal scans, the peaks always have the same fwhm, indicating that the correlation length of the different structures is the same. In this case, a value of 1000 ± 40 Å is obtained independent of the applied potential, implying that the domain size remains constant throughout the potential range where the overlayer structures are present. However, the radial scans show a clear change between the commensurate and incommensurate structures. The commensurate structure presents a much shaper and better-defined radial peak, implying that all the domains in the adlayer have the same coverage.

As aforementioned, the increase in bromide coverage associated with the phase transition is triggered by a small increase in the copper coverage on the electrode surface. To determine the species involved, the effects of copper and bromide concentrations were studied. Figure 9A shows that the peak potential shifts with the copper concentration at a rate of 32−34 mV per decade change in copper concentration, a value close to that expected for a deposition process where two electrons are exchanged (30 mV/decade). In the case of bromide, the expected value is 59 mV/decade, assuming that one electron is exchanged in the bromide adsorption process. However, a value of 11−13 mV/decade is obtained (Figure 9B). This very small value suggests that bromide is not the species that controls the peak position and that copper, on the other hand, is the species that triggers the appearance of peak I. These data confirm the role of adsorbed copper in the formation of the incommensurate

bromide structure and the phase transition. This likely results from the lowering of the work function of the gold surface induced by the deposition of small amounts of copper as described earlier.

The (4 × 4) structure is stable over the entire potential range of region b. Therefore, the bromide concentration remains constant throughout this region, in agreement with chronocoulometric measurements.[31] However, as can be seen in Figure 1, several voltammetric peaks are observed over this region, indicating that deposition processes are taking place. Since the bromide coverage is constant, peaks II and III must be associated with copper deposition. To follow the evolution of the copper coverage on the electrode surface, CTR measurements were done at three different potential values: +0.29, +0.26, and +0.17 V (Figure 6C−E). In all cases, the model employed in the fitting consisted of two layers: a copper layer adsorbed directly on the Au(111) electrode surface and a bromide layer on top of the copper layer. The bromide coverage was fixed at 0.563, the value obtained from the GIXD measurements. The parameters resulting from the fitting are shown in Table 2. As can be seen, the copper coverage increases from a value of 0.37 ± 0.05 in the valley between peaks II and III to 1 at potentials close to peak IV. From these values, we can assign peak II to the formation of a copper bromide layer, in a 1:1 ratio, and peak III to the completion of the copper layer to reach a coverage value of 1. The formation of a stoichiometric CuBr layer has been proposed previously for Cu UPD on Pt(111) electrodes in this same medium. On Pt(111) electrodes, Cu UPD presents two well-resolved peaks.[33] In the present case and after the first UPD peak, an incommensurate hexagonal structure aligned along the (1,0) surface direction is observed, corresponding to a CuBr layer with an interatomic distance of 3.74 Å.[34−36] However, the lack of resolution of peaks II and III even at very low scan rates does not allow an unambiguous characterization of the layer observed between peaks II and III as stoichiometric. However, the copper coverage values obtained in this region are close to the stoichiometric value, suggesting the formation of such a layer between the peaks. The differences in behavior between copper UPD on Pt(111) and Au(111) electrodes have been attributed to the different Au−Au and Pt−Pt distances in the (111) direction.[33]

It is also worth noting the changes in the distances between layers observed over this region. At low copper coverages, the distance between the copper and the bromide layer is almost negligible, suggesting that copper and bromide form an intermixed adlayer in which copper species occupy some interstitial spaces left by the (4 × 4) bromide structure. The distance of this mixed layer to the Au(111) surface is the same as that observed for the bromide layer in the absence of deposited copper at +0.70 V. As the copper coverage increases, a separation between the copper and bromide layers is observed. The total distance between the bromide layer and the Au(111) surface increases ($d_1 + d_2$ in Table 2) due to the presence of a separate copper layer with a diminution in $d_1$. That is, the copper layer approaches the electrode surface as its coverage increases. Finally, when the copper coverage reaches 1, two clearly separated layers are obtained with a distance between the copper and bromide layers close to that in solid CuBr.[37] This suggests that the oxidation states of the copper and bromide species in the overlayer are similar to those found in CuBr; i.e., copper has an oxidation state close to +1, whereas bromide has a charge close to −1. Similar oxidation states for copper UPD on Au(111) have been proposed in the presence of sulfate and chloride anions.[38−40]

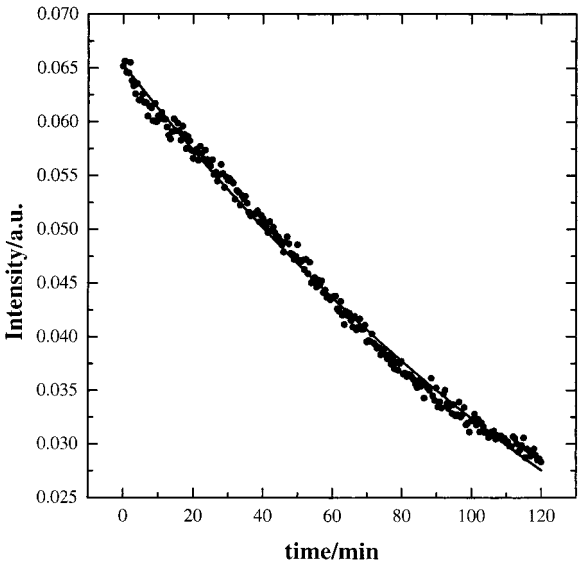


**Figure 10.** Time decay of the intensity of the diffraction peak for the (4 × 4) structure at +0.12 V (solid line is exponential fit).

**3.3. Region c.** Region c starts with peak IV (+0.147 V). As for peak I, we believe that this voltammetric feature is also associated with a phase transition. However, no other structure, different from the (4 × 4) bromide overlayer, was found at potentials below +0.147 V. If the bromide coverage does not change in this region, then copper is likely responsible for this peak. Since peak IV is close to the onset of bulk copper deposition, it could be due to a transition from a disordered copper layer to the formation of an ordered (1 × 1) layer. However, it would be quite difficult to detect a (1 × 1) copper layer from GIXD measurements since its diffraction peak would overlap that of the Au(111) surface. In addition, the intensity of the diffraction peak associated with the (4 × 4) bromide structure decreases, in an exponential fashion, with time (Figure 10) at potentials below peak I. Such a decay is likely associated with the slow bulk copper deposition that takes place at these potential values. The bulk deposition would lead to a loss in the long-range order of the surface and a diminution of the signal due to the ordered (4 × 4) structure. At these potentials, CTR measurements were not possible since the copper coverage changes with time, due to the bulk copper deposition. Although we cannot unambiguously confirm the formation of a (1 × 1) copper structure after peak IV, a phase transition in the copper overlayer to give an ordered (1 × 1) structure would be the most likely explanation for peak IV. This is also similar to other UPD systems such as Cu UPD on Pt(111) in the presence of halides such as $Cl^-$ and $Br^-$.

To confirm the involvement of copper in peak IV, studies of the effects of copper (Figure 9C) and bromide (Figure 9D) concentrations on the potential of peak IV were carried out. As Figure 9C demonstrates, the peak shifts about 30 mV/decade change in the copper concentration. This is the anticipated value for a process involving copper deposition. On the other hand, the bromide concentration has virtually no effect on the peak position, indicating that bromide is not involved in the processes that give rise to peak IV. This provides additional support for the assignment of peak IV to a phase transition of the copper layer.

## 4. Conclusions

The different structures found in the copper UPD process on Au(111) electrodes in the presence of $Br^-$ are summarized in

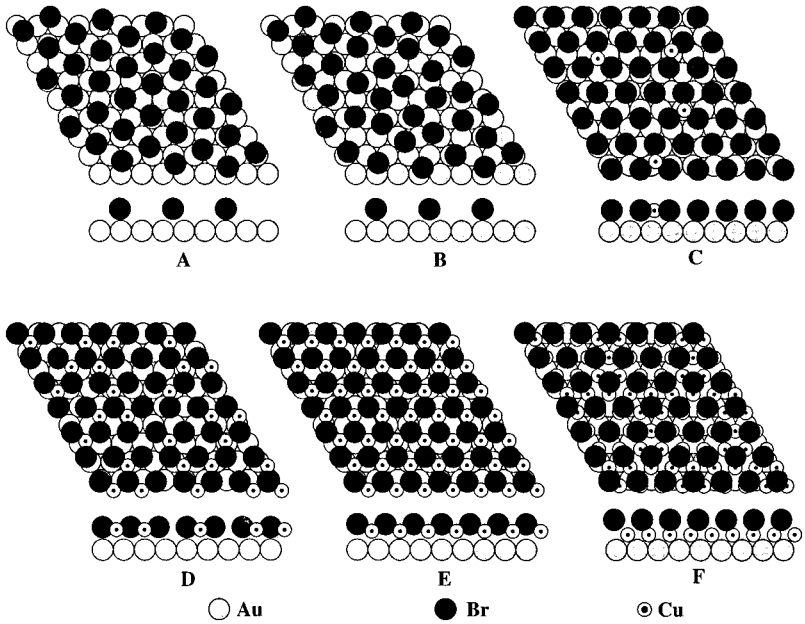


**Figure 11.** Hard ball model of the overlayer at different potential values: (A) above +0.55 V, (B) between +0.38 and +0.55 V, (C) between +0.32 and +0.36 V, (D) between +0.29 and 0.32 V, (E) at +0.29 V, and (F) below +0.14 V. For clarity, copper, gold, and bromide are not drawn to scale.

Figure 11. At potentials positive of +0.55 V, bromide adsorbs on the electrode surface, forming an ordered and rotated hexagonal structure (Figure 11A). The rotation angle of this structure with respect to the (01) direction and the Br−Br distance change with the electrode potential. At these potentials, the electrode surface is likely covered by ordered and disordered domains. The bromide coverage of the ordered domains is ca. 0.50, whereas the disordered domains have a slightly higher coverage. At potentials below +0.55 V, the bromide overlayer becomes disordered (Figure 11B), although the bromide coverage remains high.

At the shoulder of peak I, the initial stages of copper deposition lower the work function of the electrode surface, giving rise to an increase in the bromide coverage and the formation of an ordered bromide layer (Figure 11C) with a coverage of 0.51. At this point, the copper and bromide are mixed in the adlayer, with the copper atoms ostensibly occupying some interstitial holes in the hexagonal bromide structure. As the copper deposition progresses, the ordered bromide layer compresses, and a phase transition takes place at peak I to give a $(4 \times 4)$ bromide layer with a coverage of 0.563. The copper overlayer then begins to lift the bromide layer upward, and the copper layer moves closer to the Au(111) surface (Figure 11D). Between peaks II and III, the formation of a stoichiometric CuBr layer is observed (Figure 11E). Finally, after peak IV, there is a phase transition to give a $(1 \times 1)$ copper layer with a bromide $(4 \times 4)$ structure adsorbed over the copper layer (Figure 11F). At this potential, the distances between the bromide and copper layers are similar to those found in solid CuBr. At potentials negative of peak IV, the bulk copper deposition process begins.

**Acknowledgment.** This work was supported by the Office of Naval Research and the National Science Foundation. Synchrotron X-ray experiments were performed at beamline X20-C at the National Synchrotron Light Source, Brookhaven National Laboratory, which is supported by the U.S. Department of Energy, Division of Materials Science and Division of Chemical Sciences (DOE Contract DE-AC02-76CH0016). E.H. acknowledges support by a fellowship from the Ministry of Education and Science of Spain.

## References and Notes

(1) Kolb, D. M. In *Advances in Electrochemistry and Electrochemical Engineering*; Gerischer, H., Tobias, C. W., Eds.; Wiley: New York, 1978; Vol. 11, p 125.

(2) Adzic, R. In *Advances in Electrochemistry and Electrochemical Engineering*; Gerischer, H., Tobias, C. W., Eds.; Wiley: New York; Vol. 13, p 159.

(3) Matsumoto, H.; Inukai, J.; Ito, M. *J. Electroanal. Chem.* **1994**, *223*, 379.

(4) Hachiya, T.; Honbo, H.; Itaya, K. *J. Electroanal. Chem.* **1991**, *315*, 275.

(5) Sashikata, K.; Furuya, N.; Itaya, K. *J. Electroanal. Chem.* **1991**, *316*, 361.

(6) Dietterle, M.; Will, T.; Kolb, D. M. *Surf. Sci.* **1995,** *342*, 29.

(7) Chen, C.-H.; Vesecky, S. M.; Gewirth, A. A. *J. Am. Chem. Soc.* **1992**, *114*, 451.

(8) Chen, C.-H.; Kepler, K. D.; Gewirth, A. A.; Ocko, B. M.; Wang, J. *J. Phys. Chem.* **1993**, *97*, 7290.

(9) Yee, H. S.; Abruña, H. D. *Langmuir* **1993**, *9*, 2460.

(10) Gómez, R.; Yee, H. S.; Bommarito, G. M.; Feliu, J. M.; Abruña, H. D. *Surf. Sci.* **1995**, *335*, 101.

(11) Yee, H. S.; Abruña, H. D. *J. Phys. Chem.* **1993**, *97*, 6278.

(12) Wang, J. X.; Adzic, R. R.; Ocko, B. M. *J. Phys. Chem.* **1994**, *98*, 7182.

(13) Toney, M. F.; Gordon, J. G.; Samant, M. G.; Borges, G. L.; Melroy, O. R.; Yee, D.; Sorensen, L. B. *J. Phys. Chem.* **1995**, *99*, 4733.

(14) Wu, S.; Lipkowski, J.; Tyliszczak, T.; Hitchcock, A. P. *Prog. Surf. Sci.* **1995**, *50*, 227.

(15) Gómez, R.; Feliu, J. M.; Abruña, H. D. *J. Phys. Chem.* **1994**, *98*, 5514.

(16) Buller, L. J.; Herrero, E.; Gómez, R.; Feliu, J. M.; Abruña, H. D. *J. Chem. Soc., Faraday Trans.* **1996**, *92*, 3757.

(17) Samant, M. G.; Toney, M. F.; Borges, G. L.; Blum, L.; Melroy, O. R. *Surf. Sci.* **1988**, *193*, L29.

(18) Ocko, B. M.; Wang, J.; Davenport, A.; Isaacs, H. *Phys. Rev. Lett.* **1990**, *65*, 1466.

(19) Wang, J.; Ocko, B. M.; Davenport, A. J.; Isaacs, H. S. *Phys. Rev. B* **1992**, *46*, 10321.

(20) Gibbs, D.; Ocko, B. M.; Zehner, D. M.; Mochrie, S. G. J. *Phys. Rev. B* **1988**, *38*, 7303.

(21) *International Tables for X-ray Crystallography*; Ibers, J. A., Hamilton, W. C., Eds.; Kynoch: Birmingham, 1974; Vol. IV.

(22) Li, J.; Herrero, E.; Abruña, H. D. *J. Colloids Surf.*, in press.

(23) Clavilier, J.; Armand, D.; Sun, S. G.; Petit, M. *J. Electroanal. Chem.* **1986**, *205*, 267.

(24) Blum, L.; Huckaby, D. A.; Legault, M. *Electrochim. Acta* **1996**, *41*, 2207.

(25) Magnussen, O. M.; Ocko, B. M.; Adzic, R. R.; Wang, J. X. *Phys. Rev. B* **1995**, *51*, 5510.

(26) Magnussen, O. M.; Ocko, B. M.; Wang, J. X.; Adzic, R. R. *J. Phys. Chem.* **1996**, *100*, 5500.
(27) Hamelin, A.; Weaver, M. J. *J. Electroanal. Chem.* **1987**, *223*, 171.
(28) Bondi, A. *J. Phys. Chem.* **1964**, *68*, 441.
(29) Shi, Z.; Lipkowski, J. *J. Electroanal. Chem.* **1994**, *369*, 283.
(30) Shi, Z.; Wu, S.; Lipkowski, J. *Electrochim. Acta* **1995**, *40*, 9.
(31) Shi, Z.; Lipkowski, J. *J. Phys. Chem.* **1995**, *99*, 4170.
(32) Michaelson, H. B. *J. Appl. Phys.* **1977**, *48*, 4729.
(33) Herrero, E.; Glazier, S.; Abruña, H. D. *J. Electroanal. Chem.*, in press.
(34) Tidswell, I. M.; Lucas, C. A.; Markovic, N. M.; Ross, P. N. *Phys. Rev. B* **1995**, *51*, 10205.
(35) Lucas, C. A.; Markovic, N. M.; Tidswell, I. M.; Ross, P. N. *Physica B* **1996**, *221*, 245.
(36) Markovic, N. M.; Lucas, C. A.; Gasteiger, H. A.; Ross, P. N. *Surf. Sci.* **1997**, *372*, 239.
(37) Wycoff, R. W. G. *Crystal Structures*, 2nd ed.; Wiley: New York, 1963; p 110.
(38) Blum, L.; Abruña, H. D.; White, J.; Gordon II, J. G.; Borges, G. L.; Samant, M. G.; Melroy, O. R. *J. Chem. Phys.* **1986**, *82*, 6732.
(39) Tadjeddine, A.; Tourillon, G.; Guay, D. *Electrochim. Acta* **1991**, *36*, 1859.
(40) Wu, S.; Lipkowski, J.; Tyliszczak, T.; Hitchcock, A. P. *Prog. Surf. Sci.* **1995**, *50*, 227.